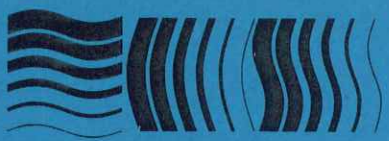

NEDERLANDSE COMMISSIE VOOR STRALINGSDOSIMETRIE
Netherlands Commission on Radiation Dosimetry

CODE OF PRACTICE FOR THE DOSIMETRY OF HIGH-ENERGY ELECTRON BEAMS

NCS REPORT 5
DECEMBER 1989

PREFACE

The Nederlandse Commissie voor Stralingsdosimetrie (Netherlands Commission on Radiation Dosimetry) was officially established on 3 September 1982 with the aim of promoting the appropriate use of dosimetry of ionizing radiation both for scientific research and practical applications. The foundation is chaired by a board of scientists installed upon the suggestion of the supporting societies including the Nederlandse Vereniging voor Radiotherapie (Netherlands Society for Radiotherapy), the Nederlandse Vereniging voor Nucleaire Geneeskunde (Netherlands Society for Nuclear Medicine), the Nederlandse Vereniging voor Klinische Fysica (Netherlands Society for Clinical Physics), the Nederlandse Vereniging voor Radiobiologie (Netherlands Society for Radiation Biology), the Nederlandse Vereniging voor Stralingshygiëne (Netherlands Society for Radiological Protection), the Kring Stralingsfysica (Netherlands Group of Radiation Physicists) and the Rijksinstituut voor Volksgezondheid en Milieuhygiëne (National Institute of Public Health and Environmental Hygiëne).
To pursue its aims the NCS accomplish the following tasks: participation in dosimetry standardisation and promotion of dosimetry intercomparisons, drafting of dosimetry protocols, collection and evaluation of physical data related to dosimetry. Furthermore the commission shall maintain or establish links with national and international organisations concerned with ionizing radiations and promulgate information on new developments in the field of radiation dosimetry.

Further copies of this report may be obtained from A.H.L. Aalbers Secretary, NCS, P.O. Box 1, 3720 BA BILTHOVEN, The Netherlands.

CODE OF PRACTICE
FOR THE DOSIMETRY OF
HIGH-ENERGY ELECTRON BEAMS

Prepared by the working party : "Uniformity Dosimetry Protocols" of the Netherlands Commission on Radiation Dosimetry (NCS) in cooperation with the Belgian Association of Hospital Physicists

Current members of the working party :

F.W. Wittkämper, Chairman
A.H.L. Aalbers
W.F.M. Brouwer
H. Huizenga
B.J. Mijnheer
A.J. Piron
S. Vynckier

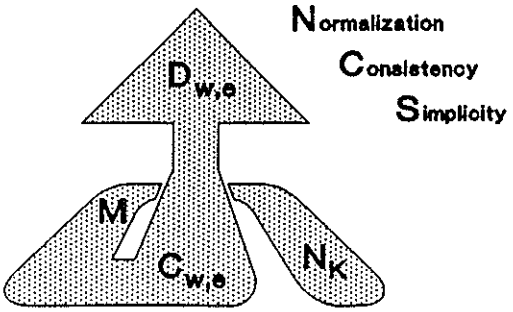

Contents

Chapter		Page
1.	Introduction	1
2.	Concept	1
3.	Code of practice	3
3.1	Definitions of the depth parameters	3
3.2	Reference chambers	3
3.3	Calibration procedure	3
3.4	Effective point of measurement	5
3.5	Determination of the range parameters	5
3.6	Mean energy at phantom surface	5
3.7	Reference conditions and reference point	6
3.8	Phantom materials and depth scaling	6
3.9	Determination of absorbed dose to water	7
3.10	$C_{w,e}$ conversion factors	8
3.11	Field instruments	8
3.12	Central axis depth dose curves	8
4.	Comments	9
4.1	Reference chambers	9
4.1.1	Choice of chamber type	10
4.2	Phantom material	11
4.2.1	Ionization correction	12
4.2.2	Depth scaling	12
4.2.3	Charge storage	13
4.3	Source-surface distance	13
4.4	Central axis ionization and depth dose curves	14
4.5	Absorbed dose as a function of field size	14
5.	General equations	16

6. Numerical values 18
6.1 Instrument reading corrections 18
6.1.1 Temperature ,pressure 18
6.1.2 Humidity 18
6.1.3 Recombination 18
6.1.3.1 Pulsed radiation 18
6.1.3.2 Pulsed-swept radiation 20
6.1.4 Polarity 21
6.2 g factor 21
6.3 k_i correction factors 22
6.3.1 k_{att} 22
6.3.2 k_m 22
6.3.3 $k_{att} * k_m$ 22
6.3.4 k_{cel} 23
6.3.5 k_{stem} 23
6.4 $s_{w,air}$ 23
6.5 p_i correction factors 24
6.5.1 p_{wall} 24
6.5.2 p_d 24
6.5.3 p_f 24
6.5.3.1 cylindrical chambers 24
6.5.3.2 NACP chamber 25
6.5.3.3 PTW/Markus chamber 25
6.5.4 p_{cel} 25
6.6 Effective point of measurement 25
6.7 Energy determination 26
6.8 Depth scaling 27
6.9 Conversion of ionization curves 27

8. References 29

1. Introduction

In the last 2 decades a number of national and international protocols and codes of practice for the dosimetry of high-energy photon and electron beams have been published. In all these protocols the formalism is based on an exposure or air kerma calibration of ionization chambers in a ^{60}Co gamma-ray or 2 MV X-ray beam. In order to derive the absorbed dose to water from an ionization chamber reading a number of correction and conversion factors have to be applied. Some of these factors were already incorporated in the early protocols (20,21,27). Between 1980 and 1984 new dosimetry protocols were issued in which more detailed knowledge of these correction and conversion factors was applied (1,22,43,53). However, different data sets for the same physical parameters (e.g. stopping powers) were employed in these protocols. In 1984 a revised set for the stopping-power data was recommended and generally adopted (29). Since then a consistent set of correction and conversion factors based on the new sets of data for the physical parameters have been established (4,5,6). To ensure consistency throughout the whole dosimetry chain the same data sets have to be used in the derivation of the exposure or air kerma at the Primary Standards Laboratory (55).

2. Concept

In 1986, the Netherlands Commission on Radiation Dosimetry [NCS] issued a code of practice for the dosimetry of high-energy photon beams (41). The numerical values were based on the most recent data for the physical parameters. In this code of practice a limited number of ionization chambers were recommended as reference chambers. In addition, the concept of single conversion factors for each of the reference chambers, as a function of the quality index of the photon beam, was applied. In these conversion factors all necessary corrections and conversions are combined. This simple approach was introduced by the HPA (23) and also adopted in Switzerland (56) and in Italy (30). If new types of ionization chambers are introduced as reference chambers, additional tables with conversion factors have to be supplied.

In 1987 the IAEA published a dosimetry protocol based on the same new and consistent data sets for the physical parameters (26). However, the concept of the Nordic and AAPM (43,1) protocols was followed. In this concept all correction and conversion factors have to be calculated or looked up from tables, separately. For this purpose worksheets are given to be filled in by the user. The advantage of this concept is that a large variety of ionization chambers can be used as reference instrument. However, such a procedure requires a thorough knowledge of the whole report, is time consuming and may be prone to errors.

Since 1 September 1987 the Primary Standards Laboratory in the Netherlands revised its air kerma value, which is now based on the new stopping-power data. By applying the NCS code of practice for photon beams, or protocols based on the same data sets, in combination with an air kerma calibration factor, consistency is now achieved in all correction and conversion factors.

The concept of single conversion factors has also been adopted in this code of practice for high-energy electron beams. This concept has shown to be the most practical one in clinical practice. In chapter 3 the procedure to derive the absorbed dose to water is described. For several ionization chambers, provided with an air kerma calibration factor obtained in a ^{60}Co gamma-ray beam, air kerma to absorbed dose to water conversion factors ($C_{w,e}$) are given as a function of the electron beam energy and depth in the phantom. Additional comments are given in chapter 4. In chapter 5 the formalism is discussed and in chapter 6 detailed information is given on the numerical values of all correction and conversion factors incorporated in this code of practice.

3. Code of practice

3.1 Definitions of the depth parameters :

$R_{100,dos}$ is the depth of maximum absorbed dose in water.
$R_{50,dos}$ is the depth in water along the central axis of the beam at which the absorbed dose is 50 % of the maximum absorbed dose.
$R_{50,ion}$ is the depth in water along the central axis of the beam at which the ionization is 50 % of the maximum ionization; see Fig. 1.
All these definitions apply for a field size of at least 10 * 10 cm^2 and an (photon) source-surface distance (SSD) of at least 100 cm (see paragraph 4.3).

3.2 Reference chambers : The absorbed dose to water at the reference point (paragraph 3.7) shall be determined with one of the following reference ionization chambers :

NE 2505/3A or NE 2571 cylindrical chambers
NACP or PTW/Markus plane-parallel chambers

From the Markus type only those manufactured by PTW* are allowed as reference instrument. This type of chamber is indicated as PTW/Markus in this code of practice. For low energies the plane-parallel chambers are recommended because the chance of introducing positioning errors and the uncertainty in some correction factors, using this type of chamber, is smaller (paragraph 4.1). The dimensions and composition of the reference chambers are given in Table I.

3.3 Calibration procedure : The reference chamber shall be calibrated in air in terms of air kerma against the National Standard or a reference chamber traceable to the National Standard in a beam of ^{60}Co gamma rays. For this calibration the cylindrical chamber shall be fitted with the build-up cap supplied with the chamber (see Table I). The plane-parallel chamber shall be calibrated with an additional layer of *0.54 gcm^{-2}* (3 mm) graphite in front of its entrance window.

* Physikalisch Technische Werkstätte

3.4 Effective point of measurement : For all measurements with an ionization chamber in an electron beam the effective point of measurement shall be used. This means, the depth of measurement in a phantom is at the depth of the effective point of measurement. For the cylindrical chambers this effective point of measurement should be taken at a fraction *0.5* of the inner chamber radius in front of its geometric center. For the plane-parallel chambers the effective point of measurement is the inner surface of the entrance window.

3.5 Determination of the range parameters : The mean energy of the electron beam at the phantom surface can be related to the depth of $R_{50,dos}$ or $R_{50,ion}$.

$R_{50,dos}$ shall be derived from the central axis depth dose curve measured with a p-type diode (paragraph 4.3) in water for a field size of at least 10 * 10 cm^2 and a source-surface distance of about 100 cm.

$R_{50,ion}$ shall be derived from the central axis depth ionization curve. This curve has to be measured with one of the reference chambers in water for a field size of at least 10 * 10 cm^2 and a source-surface distance of about 100 cm. The cylindrical chambers shall be fitted with a thin waterproofing sheath e.g. made of PMMA (Lucite, Perspex), not thicker than approximately one millimeter. For accelerators with scattering foil(s) a plane-parallel or a cylindrical reference ionization chamber can be used. For scanning electron beams a plane-parallel chamber is recommended (paragraph 4.3).

By applying this procedure no conversion from reading to dose is required for the determination of $R_{50,ion}$.

3.6 Mean energy at phantom surface : The mean energy at the phantom surface ($\bar{E}_0$) in MeV is given by

$$\bar{E}_0 = C_1 * R_{50,dos} \qquad (1)$$

or

$$\bar{E}_0 = C_2 * R_{50,ion} \qquad (2)$$

where $R_{50,dos}$ and $R_{50,ion}$ are given in centimeters. The values for C_1 and C_2 ($MeVcm^{-1}$) are given in Fig. 2 as a function of R_{50}. These relations apply for an SSD of about 100 cm.

3.7 Reference conditions and reference point : The absorbed dose shall be determined at the reference point under reference conditions.
Reference conditions : The phantom surface shall be positioned at the source-surface distance normally used. A field size of at least 10 * 10 cm^2 at either the phantom surface or the dose maximum, whichever is the normal custom, shall be used.
Reference point : The reference point is at the depth of dose maximum ($R_{100,dos}$) of the central axis depth dose curve. $R_{100,dos}$ shall be determined :
a) from the direct measurements with a p-type diode in water under the reference conditions;
b) by converting the central axis depth ionization curve, determined under the reference conditions, to the central axis depth dose curve. The central axis ionization curve shall be measured with one of the reference chambers in water. The conversion shall be done by multiplying the ionization values with the stopping power ratios water to air taken from Table II. These stopping power values are given as a function of the mean energy at the phantom surface ($\bar{E}_0$) and the depth (z). For scanning electron beams, it is recommended to use a plane-parallel ionization chamber to determine the central axis depth ionization curve (paragraph 4.3).

3.8 Phantom materials and depth scaling : The absorbed dose has to be stated to water. Besides water, PMMA (Perspex, Lucite) as phantom material is also allowed for the dose determination at the reference point. If the depth of the reference point in water is scaled to the corresponding depth in PMMA, with constant SSD, the absorbed dose to PMMA is equal to the absorbed dose to water. The corresponding depth in PMMA is determined according to the relation

$$z_{PMMA,ref} = z_{w,ref} \; / \; b_{PMMA} \qquad (3)$$

where $z_{w,ref}$ is the depth (cm) of the reference point in water and $z_{PMMA,ref}$ is the corresponding depth in PMMA (cm). b_{PMMA} is the depth scaling factor. The scaling factor depends on the densities of the PMMA phantom and water. b_{PMMA} is given by

$$b_{PMMA} = \frac{\rho_{PMMA}}{\rho_w} * csda_{w,PMMA} \qquad (4)$$

where ρ_w and ρ_{PMMA} are the densities (gcm^{-3}) of water and PMMA, respectively. $csda_{w,PMMA}$ is the ratio of the continuous-slowing-down-approximation ranges (gcm^{-2}) of water to PMMA. The value recommended for $csda_{w,PMMA}$ is *0.962*. The most common density of PMMA is 1.185 gcm^{-3} thus yielding a recommended value b_m = *1.140*. For accurate measurements the density of PMMA has to be determined.

3.9 Determination of absorbed dose to water : The ionization chamber shall be positioned with its effective point of measurement at the reference point (dose maximum). The absorbed dose to water is given by the relation

$$D_{w,e} = M * N_K * C_{w,e} \qquad (5)$$

where

$D_{w,e}$ is the absorbed dose to water in the electron beam at the position of the effective point of measurement of the chamber when the chamber is replaced by water.

M is the electrometer reading corrected for
a) any difference between the ambient air conditions affecting the chamber reading at the time of measurement and the standard ambient air conditions for which the calibration factor applies (temperature, pressure, humidity).
b) ion recombination and polarity effects in the electron beam.

N_K is the air kerma calibration factor, given by the Standards Laboratory, which converts the ionization chamber reading to air kerma for the calibration quality and geometry and for the standard air conditions (usually 22^0 C, 101.3 kPa and 50 % relative humidity).

$C_{w,e}$ is the air kerma to absorbed dose to water conversion factor, which depends on chamber type, electron beam energy and depth in the phantom.

3.10 $C_{w,e}$ conversion factors : Recommended $C_{w,e}$ values as a function of the mean energy at the phantom surface ($\bar{E}_0$) and depth in water are given in Tables III-a, III-b, and III-c for the NE 2505/3A and NE 2571, NACP and PTW/Markus ionization chamber, respectively.

3.11 Field instruments : Field instruments shall be calibrated against one of the reference chambers at the radiation quality at which they are to be used. First the absorbed dose to water shall be determined with one of the reference chambers as outlined in paragraph 3.9. Second the reading of the field instrument shall be determined with the chamber positioned in the phantom and at the depth normally used for routine output measurements. The in-phantom calibration factor at the user's beam quality, $N_{ph,e}$, is given by

$$N_{ph,e} = \frac{D_{w,e}}{M_f} = \frac{(M * N_K * C_{w,e})_{ref\ chamber}}{M_f} \qquad (6)$$

where M_f is the reading of the field instrument, corrected in a similar way as M.

3.12 Central axis depth dose curves : Central axis depth dose curves for other conditions than the reference conditions can be obtained :
a) from direct measurements with a p-type diode in water;
b) by converting central axis depth ionization curves to central axis depth dose curves. This conversion shall be done by multiplying the ionization values with the stopping power ratios water to air taken from Table II. These stopping power values are given as a function of the mean energy at the phantom surface and the depth in water. To determine the ionization curves for non-reference conditions, both the reference chambers and small cylindrical chambers with inner radii less than 3 mm can be used;
c) from measurements with film, TLD, or whatever is the normal custom in the institute. However, implementation of one of these techniques should be verified against the technique described in a or b.

4. Comments

4.1 Reference chambers : In the NCS code of practice for high-energy photon beams (41) the graphite-walled Farmer chambers (NE 2505/3A and NE 2571) and the NPL Secondary Standard ionization chamber (NE 2561) are recommended as reference chambers. Graphite is a pure material of which the dosimetry parameters (e.g. k_m) are well known. Heterogeneous chambers such as the nylon-walled Farmer chamber (NE 2505/3B) and the PMMA-walled chambers of PTW (PTW 23331, 23332, 23333) are not recommended because of the uncertainty in the k_m factor due to variations in the thickness of the graphite coating. Nowadays the NE 2505/3A, NE 2571 and NE 2561 graphite-walled Farmer chambers are used as reference chambers in all radiotherapy institutes in The Netherlands and Belgium. It is therefore advantageous to recommend the same chambers as reference chambers for the dosimetry of electron beams. However, fluence perturbation corrections are quite large for the NE 2561 chamber and have to be extrapolated from published data. These data are not verified and therefore this chamber can not be considered as a reference chamber in electron beams.
To provide $C_{w,e}$ values for the NACP and PTW/Markus plane-parallel chambers, calibrated in air kerma free in air, the ($k_{att} * k_m$) conversion factor has been determined experimentally. This conversion factor was found to be identical for individual NACP chambers (63). The polarity correction is very small for the NACP type chamber. No correction is necessary for the fluence perturbation down to at least 2 MeV energy at depth (32,64). Also for the PTW/Markus plane-parallel ionization chambers ($k_{att} * k_m$) values were found to be similar for individual chambers (63). However, the uncertainty in the average ($k_{att} * k_m$) value is somewhat larger. The polarity correction to be applied for the PTW/Markus chamber is of the same magnitude as those for the cylindrical reference chambers. Between 3 MeV and 15 MeV energy at depth an energy dependence of about 1.5 % was found (64). This energy dependence is incorporated in the $C_{w,e}$ values of the PTW/Markus chamber as a fluence perturbation correction. At this moment the $C_{w,e}$ values for the Markus chambers are only applicable to chambers which are manufactured at PTW. For Markus chambers built elsewhere first a similar type testing as performed for the PTW/Markus chambers has to be carried out. Markus chambers with serial codes beginning with an E are not suitable as reference chamber due to the large polarity correction and

energy dependence. For electron beam energies above 22 MeV no experimental data on the energy dependence of the NACP and Markus plane-parallel chambers are known at this moment. Therefore it is recommended to verify absorbed dose values determined with one of the plane-parallel chambers with one of the cylindrical reference chambers for higher energies.

4.1.1 Choice of chamber type : The electron beam energy below which plane-parallel ionization chambers are preferable to cylindrical reference chambers depends on two factors. First the uncertainty in the position of the effective point of measurement for the cylindrical chamber in relation to the shape of the central axis depth dose curve is important and second the uncertainty in the required fluence perturbation correction for the cylindrical chamber increases at lower energies. From these uncertainties two criteria can be formulated :

a) Position criterium : The NACP and PTW/Markus plane-parallel ionization chambers, with their well defined effective point of measurement, can be positioned accurately. For the cylindrical reference chambers, the position of the effective point of measurement at the depth of dose maximum is experimentally determined as a fraction of the inner radius in front of the chambers geometrical centre (31, 64). This fraction depends on the energy of the electron beam and is between 0.3 and 0.7. In this code of practice a constant value of 0.5 is recommended. If a deviation in the depth of *0.5 mm* from dose maximum decreases the measured ionization significantly, it is recommended to use one of the plane-parallel ionization chambers (see the ionization curve).

b) Energy criterium : Using the fluence perturbation corrections from Johansson et al. (31) for the cylindrical reference chambers, consistency can be achieved between absorbed dose values determined with the NACP or PTW/Markus plane-parallel chambers and the 0.6 cm^3 Farmer chambers down to a mean energy of about 3 to 4 MeV (32,64). It is recommended not to use a cylindrical chamber for mean energies at depth lower than *4 MeV*. To use this criterium the mean energy at depth can be approximately calculated with

$$\bar{E}_z = \bar{E}_0 - a * z \qquad (7)$$

where $\bar{E}_z$ is the mean energy at depth (MeV), $\bar{E}_0$ is the mean energy at the phantom surface (MeV), a is 2 MeVcm^{-1} and z is the depth (cm) in the phantom.

For some accelerators, especially those with an open collimating system and scanning electron beams, yielding rather peaked depth dose curves, the lowest energy where a cylindrical chamber is recommended may be somewhat higher than 4 MeV at depth due to the position criterium.

For the PTW/Markus chamber no experimentally verified fluence corrections are known for $\bar{E}_z$ < 2.5 MeV. Therefore this chamber can not be used for lower energies at depth.

The $C_{w,e}$ conversion factors for the NACP and PTW/Markus chambers were determined with the chambers calibrated in the ^{60}Co gamma-ray beam with and additional layer of 0.54 gcm^{-2} (3 mm) of graphite to establish electron equilibrium. If the large waterproof PMMA housing of the Scanditronix NACP chamber type 01 and the similar Dosetek plane-parallel chamber is not removed during the air kema calibration, the reading of these type of chambers will be too high due to additional scatter. This increase of reading was measured. A value of 0.4 % was found with a standard deviation of 0.1 % (63). Therefore the reading of these two types of chambers have to be multiplied with a factor of 0.996 during the air kerma calibration to correct for the waterproof PMMA housing, if not removed. The influence of the waterproof housing on the reading is negligible during the in-water measurements. Within the experimental uncertainty no differences could be observed between (k_{att} * k_m) values determined for the Scanditronix NACP chamber type 01 and type 02 and the Dosetek NACP chamber.

4.2 Phantom material : The absorbed dose has to be stated to water. However, solid phantom materials such as polymethylmethacrylate (PMMA) or polystyrene are sometimes more practical for measurements than water, especially if measurements have to be performed at a few millimeters depth or for routine measurements. To convert ionization measurements at the depth of ionization maximum in solid phantom materials to water, the measured value for the ionization has to be corrected. In addition, the depth in the solid phantom has to be scaled to the corresponding depth in

water. Whether a particular solid phantom material is suitable depends on the accuracy of the ionization correction and depth scaling.

4.2.1 Ionization correction : It can be shown that there is no significant difference between the maximum ionization measured in water and PMMA, due to the similar values for the linear scattering power for the two materials (39). Ionization measurements in polystyrene need a correction. Corrections up to 3 % have been reported, depending on the energy and type of the electron beam (15,60), although in other publications (40,43) smaller corrections, less than 1 %, are given. Therefore in this code of practice only PMMA is recommended.

4.2.2 Depth scaling : To determine the absorbed dose to water at the reference point in a PMMA phantom, the depth of the dose maximum in water has to be scaled to the corresponding depth in PMMA with the scaling factor b_{PMMA} according to equation 3. According to Markus (37) this scaling factor can be given by

$$b_{PMMA} = \frac{(Z/A)_{eff,PMMA}}{(Z/A)_{eff,w}} * \frac{\rho_{PMMA}}{\rho_w} \qquad (8)$$

where b_{PMMA} is the scaling factor as applied in equation 3, Z is the atomic number and A is the atomic mass. ρ_w and ρ_{PMMA} are the densities (gcm^{-3}) of water and PMMA, respectively. Equation 8 leads to good agreement in the absorbed dose determination between water and PMMA. For electron beam energies between 4 MeV and 20 MeV at the phantom surface, differences between the depth of the 50 % point on the central axis depth dose curve and practical range determined in water and PMMA were found to be less than 1 mm and 2 mm, respectively (40). The scaling factor adopted in this code of practice is based on the linear continuous slowing down range (r_0/ρ). According to this scaling law the linear depths in two materials, corresponding to a certain percentage depth ionization, are proportional to the continuous slowing down ranges in the two materials. In the equation

$$b_{PMMA} = \frac{(r_0/\rho)_w}{(r_0/\rho)_{PMMA}} \qquad (9)$$

$(r_0/\rho)_w$ and $(r_0/\rho)_{PMMA}$ are the linear continuous-slowing-down-ranges of water and PMMA, respectively. With this scaling factor the agreement between the percentage depth ionization in water and PMMA is even better than obtained with the scaling factor defined by equation 8 (40). In clinical practice these scaling methods can also be applied beyond the dose maximum.

4.2.3 Charge storage : Dosimetry errors can arise due to charge storage in insulating plastic phantom materials as PMMA and polystyrene irradiated with electron beams (18,19,39). According to Galbraith et al. (18) an increase in the ionization chamber reading is detectable after an absorbed dose of about 20 Gy from a 6 MeV electron beam. In these experiments 5 cm thick PMMA and polystyrene phantom blocks were used. Mattsson and Svensson (39) observed an increase of 1 % and 1.8 % of the ratio of ionization chamber measurements in PMMA to water after an accumulated dose of 100 Gy and 300 Gy, respectively. However, according to Thwaites no significant increase in chamber signal could be observed for a PMMA slab phantom consisting of slabs with thickness smaller than 2 cm (59). Also Rawlinson and colleagues concluded from calculations that charge storage is expected to be reduced if a grounded surface is relatively close to and surrrounding the grounded air cavity (48). If a PMMA phantom is used, it is therefore recommeded to have a slab phantom with slab thickness less than 2 cm. However, still attention has to be paid to possible charge storage effects e.g. by means of periodical intercomparisons with a water phantom.

4.3 Source-surface distance : The numerical values for C_1 and C_2 in equations 1 and 2 were derived from measurements with a source-surface distance of 100 cm (13). It is likely that the distance of the phantom to the photon focus was 100 cm for these measurements. Therefore, in this report with SSD is meant the photon focus-surface distance. It could be considered to use $\bar{E}_0/R_{50}$ values in relation to the virtual electron source-surface distance (28). However, differences between R_{50} determined for an SSD of 100 cm and for an infinite SSD are small for energies less than 30 MeV and will have almost no influence on the stopping-power values at dose maximum.

4.4 Central axis ionization and depth dose curves : In addition to ionization chambers, also diodes, photographic film and TLD are commonly used to determine central axis depth dose curves. Ten Haken and colleagues investigated the usefulness of these various techniques (58). All methods were found to yield reasonable results when carefully carried out, with average differences of less than one millimeter being achievable. Measurements with p-type silicon diode detectors (49) are particularly useful, as these detectors are point-like and appear to directly represent central axis depth dose data, thus requiring little or no corrections.

Central axis depth ionization curves have to be converted to central axis depth dose curves as outlined in paragraph 3.12. Some correction factors to be applied to the ionization chamber reading are dependent on depth, e.g. the recombination correction, and for cylindrical chambers also the fluence perturbation correction and the position of the effective point of measurement. These corrections are not incorporated in the conversion.

The recombination correction factor and therefore also the absolute decrease of this correction factor with depth is larger for the cylindrical reference chambers than for the plane-parallel chambers. This decrease can be up the several percent in scanning electron beams and will influence the position of $R_{50,ion}$, if not corrected for. Therefore, it is recommended to determine central axis depth ionization curves for scanning electron beams with one of the plane-parallel reference chambers.

4.5 Absorbed dose as a function of field size : The depth of dose maximum is in general dependent on field size. Using a p-type diode, the absorbed dose at dose maximum for other field sizes than the reference field size can be measured in a direct way, relative to the absorbed dose for the reference field size. Using one of the reference ionization chambers, the position of the dose maximum for other field sizes has to be determined, as outlined in paragraph 3.7. Equation 5 has to be applied for the new value of the dose maximum. For small field sizes, especially field sizes smaller than 6 * 6 cm^2, it is recommended to use a p-type diode to measure central axis depth dose curves. It is emphasized that $R_{50,dos}$, $R_{50,ion}$ have to be determined for a field size of at least 10 * 10 cm^2 and a source-surface distance of about 100 cm.

5. General equations

The formalism to derive the absorbed dose to water, based on the air kerma calibration of an ionization chamber is in its general form given by

$$D_{w,e} = M * N_K * (1-g) * \Pi k_i * s_{w,air} * \Pi p_i \qquad (10)$$

where

$D_{w,e}$ is the absorbed dose to water in the electron beam

M is the corrected instrument reading :

$$M = M_{uncorr} * p_t * p_p * p_{hum} * p_{ion} * p_{pol} \qquad (11)$$

M_{uncorr} is the uncorrected instrument reading
p_t is the air temperature correction
p_p is the air pressure correction
p_{hum} is the air humidity correction
p_{ion} is the ion recombination correction
p_{pol} is the polarity correction

N_K is the air kerma calibration factor

g is the fraction of energy of secondary charged particles converted to bremsstrahlung in air at the calibration quality.

Πk_i is the product of correction factors to be applied when the air kerma of the photon calibration beam at the absence of the chamber is related to the absorbed dose in the ionization chamber cavity :

$$\Pi k_i = k_{att} * k_m * k_{cel} * k_{stem} \qquad (12)$$

katt is a correction factor for absorption and scattering in the wall, build-up cap and central electrode of the ionization chamber in the photon calibration beam.

k_m corrects for the difference in composition between the wall plus build-up cap and air

$$k_m = [\ \alpha * s_{wall,air} * (\bar{\mu}_{en}/\rho)_{air,wall} + (1-\alpha) * s_{cap,air} * (\bar{\mu}_{en}/\rho)_{air,cap}]^{-1} \qquad (13)$$

α is the fraction of ionization due to electrons set in motion in the chamber wall.

$s_{wall,air}$, $s_{cap,air}$ are the stopping power ratios wall/air and build-up cap/air, respectively.

$(\bar{\mu}_{en}/\rho)_{air,wall}$, $(\bar{\mu}_{en}/\rho)_{air,cap}$ are the mass-energy absorption coefficient ratio air/wall and air/build-up cap, respectively.

k_{cel} corrects for the difference in composition between the central electrode and air.

k_{stem} corrects for the influence of the stem on the ionization at a particular field size.

$s_{w,air}$ is the restricted stopping-power ratio water to air.

$\Pi\ p_i$ is the product of correction factors to be applied to the measurements in the water phantom at the user's quality.

$$\Pi\ p_i = p_{wall} * p_d * p_f * p_{cel} \qquad (14)$$

p_{wall} corrects for the difference in composition between the chamber wall and water.

p_d corrects for the difference in ionization at the effective point of measurement and the depth at which the absorbed dose is stated.

p_f corrects for the fluence perturbation of the electron beam due to the presence of the air cavity in the water phantom.

p_{cel} corrects for the difference in composition between the central electrode and water.

6. Numerical values

6.1 Instrument reading corrections

6.1.1 Temperature ,pressure : Temperature and pressure corrections have to be applied if the air conditions are different from the standard air conditions (usually 22^0 and 101.3 kPa) for which the air kerma calibration factor applies (see the calibration report).

6.1.2 Humidity : For a relative humidity between 10 % and 70 % the effect of water vapor on the measured ionization can be neglected (42,46).

6.1.3 Recombination : Both for pulsed and pulsed-swept radiation the recombination in the air cavity of an ionization chamber has been studied theoretically, e.g. see Boag (9,10), Boag and Currant (11) and experimentally, e.g. see Conere and Boag (16), van Dam et al. (17), Majenka et al. (35), Marinello et al. (36) and Weinhous and Meli (61).

6.1.3.1 Pulsed radiation : The recombination in pulsed beams can be calculated if the charge density per pulse is known. The recombination correction is given by

$$(p_{ion})^{-1} = f = 1/u * \ln(1+u) \qquad (15)$$

with

$$u = \frac{\mu \; m \; d^2}{V} \qquad (16)$$

where m is the charge density (Cm^{-3}), d is the electrode spacing of the ionization chamber (m), V is the collecting voltage across the chamber (V) and μ is a constant with the value of $3.02 * 10^{10}$ VmC^{-1} (11). For m given in cGy per pulse and d given in mm then μ = 10.64 $Vmm^{-2}cGy^{-1}$. For cylindrical chambers the effective electrode spacing can be calculated from

$$d_{cyl} = (r_e - r_i) * k_{cyl} \qquad (17)$$

with

$$k_{cyl} = \left[\frac{r_e+r_i}{r_e-r_i} * \frac{\ln(r_e/r_i)}{2} \right]^{1/2} \quad (18)$$

where r_e and r_i are the radii of the air cavity and central electrode, respectively.

The recombination correction can also be determined experimentally using the two-voltage method as described by Boag and Currant (11). From two ionization chamber readings with different voltages the recombination can be calculated. To simplify the calculations, Weinhous and Meli (61) have computed quadratic fit coefficients as a function of the voltage ratio. The recombination can be calculated with

$$p_{ion} = a_0 + a_1*(M_1/M_2) + a_2*(M_1/M_2)^2 \quad (19)$$

where M_1 and M_2 are the ionization chamber readings at a voltage V_1 and V_2, respectively. p_{ion} is the recombination correction to be applied with the voltage V_1. In Table (Va) the coefficients are given as a function of V_1/V_2. A voltage ratio equal to or greater than 3 is recommended.

6.1.3.2 Pulsed-swept radiation : The radial variation in the intensity of a scanning electron beam can be fitted by a gaussian curve. The charge density m is given by

$$m = M * \exp(-r^2/a^2) \quad (20)$$

where M is the charge density produced when the beam axis points directly at the chamber, r is the distance of the axis of the scanning beam to the ionization chamber and a is the scale constant of the gaussian distribution. The collection efficiency is a complex function of $\mu Md^2/V$, where μ, d and V have the same meaning as in paragraph. 6.1.3.1. From Boag's theory follows a relation between M and the charge measured with a chamber exposed for a time near the centre of a field scanned by an electron beam. If the scale constant, the pulse repetition frequency of the scanning beam and the exposure time are known, p_{ion} can be calculated in an iterative process [Boag (10)].

More useful in clinical practice is the procedure in which the recombination correction is determined using the two-voltage method, as described by Boag (10).In an iterative proces the recombination correction can be calculated from two measurements with different voltages. To

simplify the calculations, Weinhous and Meli (61) have also computed quadratic fit coefficients as a function of the voltage ratio for this situation, analogous to eguation (19). In Table (Vb) these coefficients are given as a function of V_1/V_2. A voltage ratio equal to or greater than 3 is recommended.

The quadratic fit coefficients are computed with the assumption that the scale constant is small compared to the field size (e.g. scale constant less than a quarter of the field size). Recombination corrections for the reference chambers exposed to a scanning electron beam (Sagittaire) have also been calculated taking into account the actual beam width. Values for the gaussian beam width were taken from Huizenga and Storchi (25). The differences were very small; in most cases less than 0.1 %. Therefore the influence of the beam width can be neglected for the reference chambers under normal operating conditions.

6.1.4 Polarity : The polarity correction for the NACP type chamber is generally small (< 0.5 %). For the cylindrical and PTW/Markus reference chambers the polarity correction can be up to 1 to 2 % for low energy electron beams. The polarity effect shall be measured for each individual reference chamber at the reference point in the energy range where the chamber is applied. Also for relative measurements with field instruments the polarity correction has to be determined at the energies where the chamber is to be used. If the polarity correction is more than a few percent, the chamber is not recommended for electron beam dosimetry. The polarity correction is defined as :

$$p_{pol}^{+} = \frac{|M^{+}| + |M^{-}|}{2 * |M^{+}|} \qquad p_{pol}^{-} = \frac{|M^{+}| + |M^{-}|}{2 * |M^{-}|} \tag{21}$$

where M^{+} and M^{-} are the ionization chamber readings at the reference point for a positive and negative chamber voltage, respectively. p_{pol}^{+} and p_{pol}^{-} are the corrections to be applied to the ionization chamber signal for a positive and negative chamber voltage, respectively.

6.2 g factor : The most recent calculation of the fraction of energy of secondary charged particles that is converted to bremsstrahlung in air amounts for ^{60}Co gamma rays to 0.003 (12).

6.3 k_i correction factors : A formal derivation of the correction factors to be applied for thick-walled ionization chambers in photon beams is given by Bielajew (8).

6.3.1 k_{att} : The correction factor k_{att} consists of two factors; k_{ab} which represents the fractional decrease in the ionization chamber response due to absorption of the primary ^{60}Co gamma-ray beam in the chamber and k_{sc} which represents the fractional increase in the response due to scattered photons (50). For the two cylindrical reference chambers a k_{att} value of 0.990 was derived from Monte Carlo calculations performed by Nath and Schulz (46) and Rogers et al. (50). Also the experimentally determined values of Johansson et al. (31) for the NE 2505/3A Farmer chamber yield the same value. For the NACP and PTW/Markus plane-parallel chambers no data are available at this moment. Monte Carlo calculations by Nath and Schulz for plane-parallel chambers are based on equal wall thickness for front and back walls, whereas for the NACP and Markus plane-parallel chambers back wall materials are much thicker resulting in a larger backscatter component.

6.3.2 k_m : Values for this quantity have been calculated for the cylindrical reference chambers by applying equation 13. The $s_{wall,air}$ and $s_{cap,air}$ values are based on values given in ICRU Report 37 (29) and are provided by Andreo et al. (4). Mass-energy absorption coefficients have been taken from Hubbell (24). Values for α were adopted from Lempert et al. (34). The calculated data for the cylindrical chambers are summarized in reference 58 and are in agreement with data calculated by Andreo et al. (5). For the NACP and PTW/Markus plane-parallel chambers k_m values can not be calculated at this moment due to the heterogeneity of the chamber wall materials (Nilsson (47), Wittkämper et al. (63)).

6.3.3 $k_{att} * k_m$: For the reference chambers $k_{att} * k_m$ values were determined experimentally relative to the $k_{att} * k_m$ value for the NE 2505/3A reference chamber provided with a graphite build-up cap in a high energy electron beam (62,63). The values adopted in this code of practice are summarized in Table IV. For the cylindrical chambers the average of calculated and measured data were taken. The mean value of $k_{att} * k_m$ for the NE 2505/3A chamber differs 0.1 % with the value for the NE 2571

chamber. In this code of practice the $k_{att} * k_m$ for the NE 2571 chamber was taken for both chambers.

6.3.4 k_{cel} : Values for the central electrode correction in the ^{60}Co gamma-ray calibration beam for the cylindrical chambers with electrodes made of aluminium were taken from Rogers et al. (50). For both chambers a value of 1.008 was adopted. This value is in close agreement with the experimental values of Mattsson (38) and Kristensen (33) and calculations performed by Nahum (44).

6.3.5 k_{stem} : Stem corrections for the reference chambers and reference field size are generally very small and can be neglected. However, an inspection of the existence of small cavities in the stem (e.g., by means of a radiograph) is recommended.

6.4 $s_{w,air}$: The restricted collision mass stopping-power data water to air used in this code of practice have been taken from the AAPM protocol (1). These data are based on Monte Carlo calculations of Berger for mono-energetic broad electron beams perpendicularly incident on a water phantom. Stopping-power data were taken from ICRU 37 (29) and were calculated according to the Spencer-Attix formulation of the Brag-Gray cavity theory with Δ = 10 keV. Andreo and colleagues (7) have studied the influence of the energy and angular spread on the stopping power ratios water to air. For the extreme situation that simulates the highest low-energy electron contamination and widest energy distribution and angular spread existing in a clinical beam, a maximum difference of 1 % occurs between the stopping power values of this clinical beam and a mono-energetic beam with the same mean energy at phantom surface at depths between 0 to 3.5 cm. At dose maximum this difference is 0.5 %. For an energy spread of 0.5 MeV and angular spread of 5^0, which are normal values in clinical electron beams, the stopping power ratios water to air agree within 0.5 % with the stopping power ratios for mono-energetic beams over the clinically useful depth interval. At the depth of dose maximum the difference is only 0.2 %. These differences are smaller than the uncertainty in the stopping power values. At the depths of therapeutic interest the stopping power ratios for mono-energetic beams can therefore be applied. At large depth an overestimation of the stopping power ratio of a few percent can occur but this has only a

small influence on the shape of the tail of the depth dose curve. The stopping-power data incorporated in the $C_{w,e}$ values are given in Table II.

6.5 p_i correction factors

6.5.1 p_{wall} : Nahum has given a theoretical treatment of the influence of the wall material on the ionization in the air cavity (44). The conclusions are that the effect is generally less than 0.5 % for common wall materials. Also Almond and Svensson concluded that for relatively thin (i.e. less then 0.5 mm) chamber walls made of low atomic number materials the influence of the difference between the wall material and water on the measured ionization is small (2). In this code of practice the p_{wall} effect is neglected.

6.5.2 p_d : The reference chambers have to be positioned with their effective point of measurement at the reference point (dose maximum). The displacement correction is one at this position.

6.5.3 p_f : Fluence perturbation corrections are necessary to account for unbalance between the number of electrons scattered from the adjacent phantom material into the air cavity and the number of electrons scattered out by the air cavity. Also the overall track length of electrons in the air cavity volume will be different from the overall track length in a similar volume of phantom material. Both processes are due to differences in scattering power of air and of the phantom material.

6.5.3.1 cylindrical chambers : Correction factors for the fluence perturbation of cylindrical chambers were determined experimentally by Johansson et al. (31). The correction factor depends on the mean energy at depth ($\bar{E}_z$) and the radius of the ionization chamber. In this report the mean energy at depth was derived from recent data provided by Andreo and Brahme (3). If the mean energy at depth calculated by Johansson is different from the mean energy at depth calculated from the data provided by Andreo and Brahme, it will influence the p_f data of Johansson et al. In this code of practice fluence perturbation correction values were used, derived from recent measurements by Wittkämper et al. (64). Partial linear and partial exponential curve fitting was applied to interpolate between and extrapolate from the data. The relations are given by

$\bar{E}_z$ < 12 MeV $\quad p_f = 0.952 + 0.0028*\bar{E}_z$ (22)

$\bar{E}_z$ ⩾ 12 MeV $\quad p_f = 1 - 0.18*\exp(-0.21*\bar{E}_z)$ (23)

6.5.3.2 NACP chamber : According to Mattsson et al. (40) no fluence perturbation correction is needed for the NACP plane-parallel chamber due to its construction and width of the guard ring. This has been confirmed experimentally by Johansson (32) and Wittkämper et al. (64).

6.5.3.3 PTW/Markus chamber : For the PTW/Markus chamber an energy dependence was found in the energy region between 3 MeV and 14 MeV at depth as discussed extensively elsewhere (64). In this code of practice the following exponential curve fitting is adopted

$$p_f = 1 - 0.041 * \exp(-0.40 * \bar{E}_z) \quad (24)$$

For $\bar{E}_z$ < 2.5 MeV no experimental data are available. Therefore $C_{w,e}$ values are not given for lower energies at depth.

In Fig. 3 the p_f values adopted in this code of practice for the reference chambers are shown as a function of the mean energy at depth.

6.5.4 p_{cel} : Both from theory and from experiments performed by Mattsson (38), it can be concluded that in electron beams there is no difference in response between chambers having graphite or aluminium central electrodes. Therefore, the value of p_{cel} for the Farmer chambers was taken unity.

6.6 Effective point of measurement : The effective point of measurement for the NACP and PTW/Markus plane-parallel chambers is at the inner surface of the entrance window. For the NACP chamber this window is made of 0.5 mm graphite covered with a 0.1 mm Mylar waterproofing sheet. The PTW/Markus chamber has an entrance window made of 2.3 $mgcm^{-2}$ polyethylene. For the cylindrical chambers the position of the effective point of measurement is a function of the electron beam energy and depth in the phantom. Its recommended position is a factor 0.5 * inner radius in front of the geometrical centre. This value is taken from data of Johansson et al. (31) and applies for the ionization maximum. (See also paragraph 4.1).

6.7 Energy determination : The air kerma to absorbed dose to water conversion factor ($C_{w,e}$) is a function of the mean energy at the phantom surface and depth. The mean energy at the phantom surface is calculated in this code of practice from the 50 % depth in water of the central axis depth dose curve ($R_{50,dos}$) or the central axis depth ionization curve ($R_{50,ion}$). Brahme and Svensson (13) showed from measurements on different medical accelerator beams that $R_{50,dos}$ in water is approximately related to the mean electron energy at phantom surface by

$$\bar{E}_0 = C_3 * R_{50,dos} \qquad (25)$$

with C_3 is 2.33 $MeVcm^{-1}$. This value is only valid in the energy range 5 to 35 MeV and for broad beams perpendicular incident on a water phantom. If $R_{50,dos}$ is determined for an SSD down to 100 cm this relation holds to a maximum energy of 20 MeV (28). Above this energy an inverse square law correction has to be made on the depth of $R_{50,dos}$. If R_{50} is determined from the depth ionization curve, Wu and colleagues suggested a value of 2.38 $MeVcm^{-1}$ for C_3 in the energy range from 5 to 50 MeV and for an infinite SSD (65). If R_{50} is determined with an finite SSD, inverse square law correction have to be made. A method, using the virtual source surface distance (28), is described by Schulz et al. (54) and Ten Haken et al. (57). However, a R_{50} to energy conversion value based on $R_{50,dos}$ or $R_{50,ion}$ determined with an SSD of 100 cm is more practical. In the NACP protocol (43) the relations between E_0 and R_{50} determined from the depth dose curve ($R_{50,dos}$) and depth ionization curve ($R_{50,ion}$) for an SSD of 100 cm are tabulated. From this table conversion values (C_1 and C_2) were derived. These values are given in Fig. 2 and Fig. 4. Ten Haken and colleagues have studied the relation between $R_{50,ion}$ with an SSD of 100 cm and $R_{50,dos}$ with infinite SSD (57). Rogers et al. determined the relation between $R_{50,dos}$ for infinite SSD and $\bar{E}_0/R_{50,dos}$ determined with Monte Carlo methods, using the ETRAN code and the EGS4 code (51), From these two relations, C values for $R_{50,ion}$ with an SSD of 100 cm could be derived. These data are also depicted in Fig. 4. The values based on the ETRAN code are in agreement with the data based on the NACP protocol. In this code of practice only the C values based on the NACP data are used. The two graphs given in Fig. 2 and Fig. 4 are best fits to the NACP data. From these graphs the C_1 and C_2

values in equation 1 and 2, respectively can be derived. The values are valid only for R_{50} values determined for a field size of at least 10 * 10 cm^2 and a source-surface distance of 100 cm.

6.8 Depth scaling : The scaling factor to be applied when PMMA is used as phantom material is in this code of practice the ratio of the linear continuous-slowing-down range of water to PMMA.

$$b_{PMMA} = \frac{(r_0/\rho)_w}{(r_0/\rho)_{PMMA}} \qquad (26)$$

where $(r_0/\rho)_w$ and $(r_0/\rho)_{PMMA}$ are the linear continuous-slowing-down ranges of water and PMMA, respectively. In ICRU Report 35 continuous-slowing-down-approximation (csda) values are given in gcm^{-2} (28). b_{PMMA} is therefore separated into two parts

$$b_{PMMA} = \frac{r_{0,w}}{r_{0,PMMA}} * \frac{\rho_{PMMA}}{\rho_w} = csda_{w,PMMA} * \frac{\rho_{PMMA}}{\rho_w} \qquad (27)$$

where $r_{0,w}$ and $r_{0,PMMA}$ are the csda values (gcm^{-2}) of water and PMMA, respectively. ρ_w and ρ_{PMMA} are the densities (gcm^{-3}) of water and PMMA, respectively. $csda_{w,PMMA}$ is the ratio of the continuous slowing-down-approximation ranges of water to PMMA. $r_{0,w}$ and $r_{0,PMMA}$ are a function of the energy of the electrons, for which the mean energy at the phantom surface (E_0) was chosen. $csda_{w,PMMA}$ is plotted in Fig. 5 as a function of the energy (MeV). As can be seen, the energy dependence of $csda_{w,PMMA}$ over the energy range covered by this code of practice is small. At a depth of 10 mm in the PMMA phantom, a variation of 1 % in the csda ratio results in a variation in depth in water of 0.1 mm. For simplicity a single value of 0.962 has been chosen in this code of practice. The most common density of PMMA is 1.185 gcm^{-3}; For accurate measurements the density of the PMMA phantom has to be determined.

6.9 Conversion of ionization curves : Central axis depth ionization curves have to be converted to central axis depth dose curves by multiplying the ionization values with the stopping power ratios water to air taken from Table II. If central axis depth ionization curves have been measured with a plane-parallel chamber the depth dependence of the recombination correction

has to be taken into account. However, for the reference plane-parallel chambers this is only a small correction and has almost no influence on the depth and shape of the ionization curve for accelerators with scattering foils. For scanning electron beams the variation of the recombination correction with depth in the phantom might have a small influence on the exact shape of the curve. For cylindrical chambers, in principle the depth dependence of the fluence perturbation, recombination correction and position of the effective point of measurement have to be taken into account. If a cylindrical chamber with a small diameter (radius < 2 mm) is used to measure the ionization curve, the variation of these corrections with depth will have only a minor influence on the position and shape of the curve if not corrected for. However, it is recommended to compare central axis depth dose curves determined with cylindrical chambers with curves determined with plane-parallel chambers or p-type diodes.

8. References

1 AAPM (American Association of Physicists in Medicine). A protocol for the determination of absorbed dose from high-energy photon and electron beams. Med. Phys. 10: 741-771, 1983.

2 Almond, P.R. and Svensson, H. Ionization dosimetry for photon and electron beams. Acta Radiol. Ther. Phys. Biol. 16: 177-186, 1977.

3 Andreo, P. and Brahme, A. Mean energy in electron beams. Med. Phys. 8: 682-687, 1981.

4 Andreo, P. and Brahme, A. Stopping power data for high-energy photon beams. Phys. Med. Biol. 31: 839-858, 1986.

5 Andreo, P., Nahum, A. and Brahme, A. Chamber-dependent wall correction factors in dosimetry. Phys. Med. Biol. 31: 1189-1199, 1986.

6 Andreo, P., Nahum, A.E. and Svensson, H. Recent developments in basic dosimetry. Radiother. Oncol. 10: 117-126, 1987.

7 Andreo, P., Brahme, A., Nahum, A.E. and Mattsson, L.O. Influence of energy and angular spread on stopping-power ratios for electron beams. Phys. Med. Biol. 34: 751-768, 1989.

8 Bielajew, A.F. Ionization cavity theory: a formal derivation of perturbation factors for thick-walled ion chambers in photon beams. Phys. Med. Biol. 31: 161-170, 1986.

9 Boag, J.W. Ionization measurements at very high intensities. 1. Pulsed radiation beams. Br. J. Radiol. 23: 601-611, 1950.

10 Boag, J.W. The recombination correction for an ionization chamber exposed to pulsed radiation in a 'swept beam' technique. 1. Theory. Phys. Med. Biol. 27: 201-211, 1982.

11 Boag, J.W. and Currant, J. Current collection and ionic recombination in small cylindrical ionization chambers exposed to pulsed radiation. Br. J. Radiol. 53: 471-478, 1980.

12 Boutillon, M. Values of g for photon energies. CCEMRI Report (1)/85-18. Offilib, Paris, 1985.

13 Brahme, A. and Svensson, H. Specification of electron beam quality from the central-axis depth absorbed dose distribution. Med. Phys. 3: 95-102, 1976

14 Brahme, A. and Svensson, H. Radiation beam characteristics of a 22 MeV microtron. Acta Rad. Oncol. 18: 244-272, 1979.

15 Bruinvis, I.A.D., Heukelom, S. and Mijnheer, B.J. Comparison of ionization measurements in water and polystyrene for electron beam dosimetry. Phys. Med. Biol. 30: 1043-1053, 1985.

16 Conere, T.J. and Boag, J.W. The collection efficiency of an ionization chamber in a pulsed and magnetically swept electron beam: Limits of validity of the two-voltage technique. Med. Phys. 11: 465-468, 1984.

17 Dam, J van., Rijnders, A., Ang, K.K., Mellaerts, M. and Grobet, P. Determination of ionization chamber collection efficiency in a swept electron beam by means of thermoluminescent detectors and the "two-voltage" method. Radiother. Oncol. 3: 363-370, 1985.

18 Galbraith, D.M., Rawlinson, J.A. and Munro, P. Dose errors due to charge storage in electron irradiated plastic phantoms. Med. Phys. 11: 197-203, 1984.

19 Ho, A.K., Paliwal, B.R. and Attix, F.H. Charge storage in electron-irradiated phantom materials. Med. Phys. 13: 99-100, 1986.

20 HPA (Hospital Physicists Association). A Code of practice for the dosimetry of 2 to 8 MV X-ray and ^{137}Cs and ^{60}Co gamma-ray beams. Phys. Med. Biol. 9: 457-463, 1964.

21 HPA (Hospital Physicists Association). A Code of practice for the dosimetry of 2 to 35 MV X-ray and ^{137}Cs and ^{60}Co gamma-ray beams. Phys. Med. Biol. 14: 1-8, 1969.

22 HPA (Hospital Physicists Association). Revised code of practice for the dosimetry of 2 to 25 MV x-ray, and of caesium-137 and cobalt-60 gamma-ray beams. Phys. Med. Biol. 28: 1097-1104, 1983.

23 HPA (Hospital Physicists Association). Code of practice for electron beam dosimetry. Phys. Med. Biol. 30: 1169-1194, 1985.

24 Hubbell, J.H. Photon mass attenuation and energy-absorption coefficients from 1 keV to 20 MeV. Int. J. Appl. Radiat. Isot. 33: 1269-1290, 1982.

25 Huizenga. H. and Storchi, P.R.M. The in-air scattering of clinical electron beams as produced by accelerators with scanning beams and diaphragm collimators. Phys. Med. Biol. 8: 1011-1029, 1987.

26 IAEA (International Atomic Energy Agency). Absorbed dose determination in photon and electron beams. Technical reports series no. 277, Vienna, 1987.

27 ICRU (International Commission on Radiation Units and Measurements). Radiation dosimetry :X rays and gamma rays with maximum photon energies between 0.6 and 50 MeV, Report 14. ICRU publications, Bethesda, Maryland, U.S.A., 1964.

28 ICRU (International Commission on Radiation Units and Measurements). Radiation dosimetry: Electron beams with energies between 1 and 50 MeV. Report 35. ICRU publications, Bethesda, Maryland, U.S.A., 1984.

29 ICRU (International Commission on Radiation Units and Measurements). Stopping powers for electrons and positrons, Report 37. ICRU publications, Bethesda, Maryland, U.S.A., 1984.

30 Italian protocol for photon and electron dosimetry in radiotherapy. Sub-Committee for Basic Dosimetry, Committee for Standardization of Dosimetry in radiotherapy, Italian Association of Biomedical Physicists (AIFB).

31 Johansson, K.A., Mattsson, L.O., Lindborg, L. and Svensson, H. Absorbed dose determination with ionization chambers in electron and photon beams having energies between 1 and 50 MeV. In proceedings National and International Standarization of Radiation Dosimetry, IAEA-SM-222/35, 243-270, International Atomic Energy Agency, Vienna, 1978.

32 Johansson, K.A. Studies of different methods of absorbed dose determination and a dosimetric intercomparison of the Nordic radiotherapy centres. Thesis University of Göteborg, 1982.

33 Kristensen, M. Measured influence of the central electrode diameter and material on the response of a graphite ionization chamber to ^{60}Co gamma rays. Phys. Med. Biol. 28: 1269-1278, 1983.

34 Lempert, G.D., Nath, R. and Schulz, R.J. Fraction of ionization from electrons arising in the wall of an ionization chamber. Med. Phys. 10: 1-3, 1983.

35 Majenka, I., Rostkowska, J., Derezinski, M. and Paz, N. The recombination correction for an ionization chamber exposed to pulsed radiation in a 'swept beam' technique. 2. Experimental. Phys. Med. Biol. 27: 213-221, 1982.

36 Marinello, G., Valero, M. and Bellec-Pollack, J. The study of a swept electron beam in order to apply Boag's theory for calculation of the collection efficiency: 2 Application to different ionization chambers and comparison with other methods. Phys. Med. Biol. 31: 869-878, 1986.

37 Markus, B. Energiebestimmung schneller Elektronen aus tiefendosiskurven. Strahlentherapie 116: 280, 1961.

38 Mattsson, L.O. Application of the water calorimeter, Fricke dosimeter and ionization chamber in clinical dosimetry. Thesis, University of Göteborg, Sweden, 1984.

39 Mattsson, L.O. and Svensson, H. Charge build-up effectc in insulating phantom materials. Acta Rad. Oncol. 23: 393-399, 1984.

40 Mattsson, L.O., Johansson, K.A. and Svensson, H. Calibration and use of plane-parallel ionization chambers for the determination of absorbed dose in electron beams. Acta Rad. Oncol. 20: 385-399, 1981.

41 Mijnheer, B.J., Aalbers A.H.L., Visser, A., and Wittkämper, F.W. Consistency and simplicity in the determination of absorbed dose to water in high-energy photon beams: a new code of practive (NCS Report 2). Radiother. Oncol. 7: 371-384, 1986.

42 Mijnheer, B.J. and Williams, J.R. Comments on dry air or humid air values for physical parameters used in the AAPM protocol for photon and electron dosimetry. Med. Phys. 12: 656-658, 1985.

43 NACP (Nordic Association of Clinical Physics) Procedures in external radiation therapy with electron and photon beams with maximum energies between 1 and 50 MeV. Acta Radiol. Oncol. 19: 55-79, 1980.

44 Nahum, A.E. Extension of the Spencer-Attix cavity theory to 3-media situation for electron beams. Proc. Symp. Int. Atomic Energy Agency (IAEA-SM-298/81), 1: 87-115, 1988.

45 Nahum, A.E., Thwaites, D.I. and Andreo, P. An analysis of the revised HPA dosimetry protocols. Phys. Med. Biol. 33: 923-938, 1988.

46 Nath, R. and Schulz, R.L. Calculated response and wall correction factors for ionization chambers exposed to ^{60}Co gamma rays. Med. Phys. 8: 85-93, 1981.

47 Nillsson, B. Private communication, 1987.

48 Rawlinson, J.A., Bielajew, A.F., Munro, P. and Galbraith, M. Theoretical and experimental investigation of dose enhancement due to charge storage in electron-irradiated phantoms. Med. Phys. 11: 814-821, 1984.

49 Rikner, G. Characteristics of a p-Si detector in high-energy electron fields. Acta Radiol. Oncol. 24: 71-74, 1985.

50 Rogers, D.W.O., Bielajew, A.F. and Nahum, A.E. Ion chamber response and A_{wall} correction factors in a ^{60}Co beam by Monte Carlo simulation. Phys. Med. Biol. 30: 429-443, 1985.

51 Rogers, D.W.O. and Bielajew, A.F. Differences in electron depth-dose curves calculated with EGS and ETRAN and improved energy-range relationships. Med. Phys. 13: 687-694, 1986.

52 Rogers, D.W.O. and Ross, C.K. The role of humidity and other correction factors in the AAPM TG-21 dosimetry protocol. Med. Phys. 15: 40-48, 1988.

53 SEFM (Sociedad Española de Fisica Medica). Procedimientos Recomendados para la Dosimetria de Fotones y Electrones de Energias Comprendidas entre 1 MeV y 50 MeV en Radioterapia de Haces Extraños, SEFM publication No. 1/1984, Comite de Dosimetria en Radioterapia, Madrid (1984).

54 Schulz, R.J. and Meli, J.A. Reply to comments of Wu et al. Med. Phys. 11: 872-874, 1984.

55 Svensson, H. The new NACP- and ICRU-dosimetry protocols for dosimetry of high-energy photon and electron radiation. Radioth. Oncol. 4: 291-294, 1985.

56 Swiss Society of Radiation Biology and Radiation Physics. Dosimetry of high energy photon and electron beams, 1986. Correspondence G. Garavaglia, Ospedale San Giovanni, 6500 Bellinzona, Switserland.

57 Ten Haken, R.K., Fraass, B.A. and Jost, R.J. Determination of electron beam mean energy from d_{50} (ionization). Med. Phys. 14: 985-991, 1987.

58 Ten Haken, R.K., Fraass, B.A. and Jost, R.J. Practical methods of electron depth-dose measurements compared to use of the NACP design chamber in water. Med. Phys. 14: 1060-1066, 1987.

59 Thwaites, D.I. Charge storage effect on dose in insulating phantoms irradiated with electrons. Phys. Med. Biol. 29: 1153-1156, 1984.

60 Thwaites, D.I. Measurement of ionization in water, polystyrene and a 'solid water' phantom material for electron beams. Phys. Med. Biol. 30: 41-53, 1985.

61 Weinhous. M.S. and Meli, A.M. Determinating p_{ion}, the correction factor for recombination losses in an ionization chamber. Med. Phys. 11: 846-849, 1984.

62 Wittkämper, F.W. and Mijnheer, B.J. Experimental determination of wall correction factors; Part 1 : cylindrical ionization chambers. Submitted for publication to Phys. Med. Biol.

63 Wittkämper, F.W., Mijnheer, B.J. and Aalbers, A.H.L. Experimental determination of wall correction factors; Part 2 : plane-parallel ionization chambers. Submitted for publication to Phys. Med. Biol.

64 Wittkämper, F.W., Thierens, H., van der Plaatsen, A. and Mijnheer, B.J. Fluence perturbation corrections for cylindrical and plane-parallel ionization chambers. To be published.

65 Wu, A., Kalend, A.M., Zwicker, R.D. and Sternick, E.S. Comments on the method of energy determination for electron beams in the TG-21 protocol. Med. Phys. 11: 871-872, 1984.

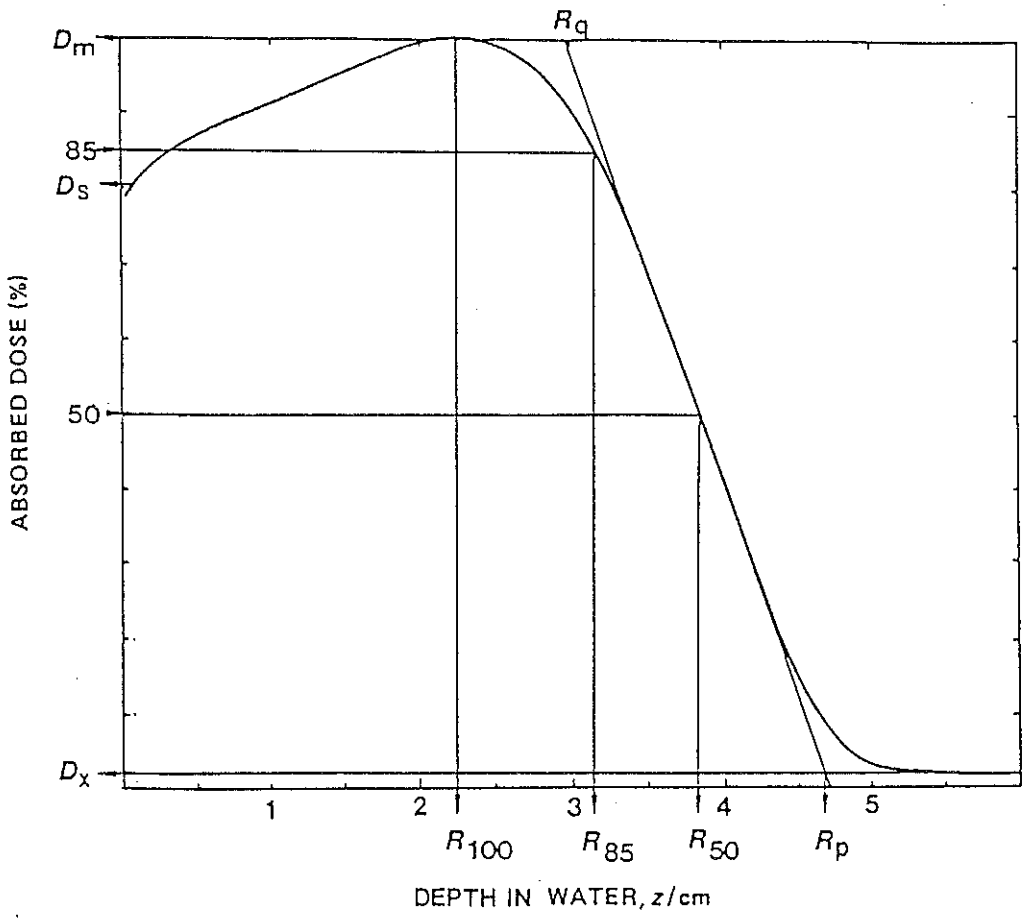

Fig. 1 Characteristic central axis depth dose distribution in water of an electron beam showing the various parameters (taken from Brahme and Svensson (13)). R_{100} is the depth of the dose maximum, R_{85} and R_{50} are the depths of the 85 % and 50 % of the maximum dose, respectively, R_p is the practical range and R_q is the depth where the tangent at the steepest point intersects the maximum absorbed dose level (D_m). A normalized dose gradient G is recommended as measure of the fall-off of the depth vs. absorbed dose distribution beyond the therapeutic range (R_{85}). G is defined as $R_p/(R_p-R_q)$.

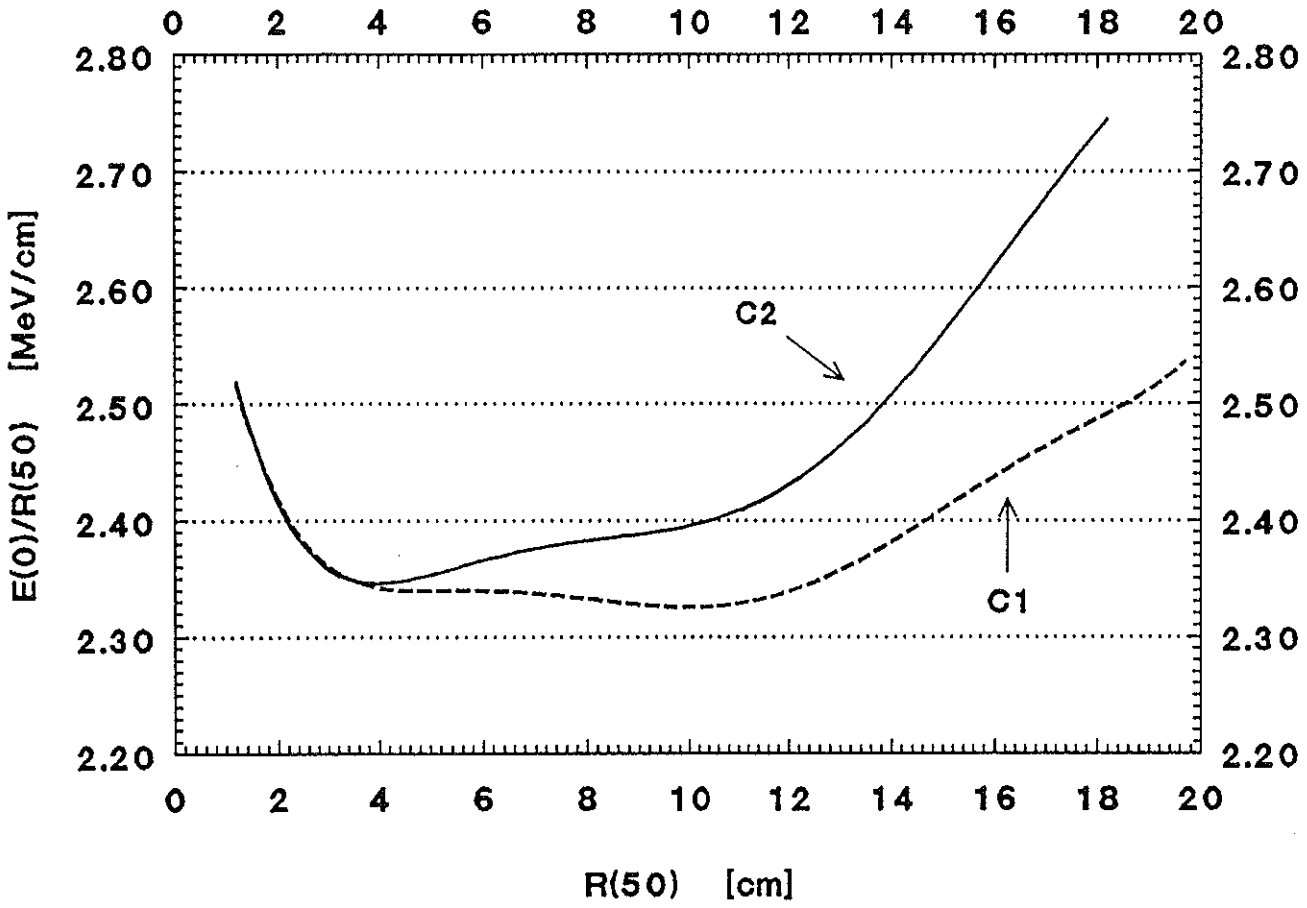

Fig. 2 $\bar{E}_0/R_{50}$ conversion factors (MeV/cm) as function of the R_{50} depth (cm) in water. The solid line is valid for R_{50} taken from the depth ionization curve for SSD=100 cm ($R_{50,ion}$). The dashed curve is valid for R_{50} taken from the depth-dose curve for SSD=100 cm ($R_{50,dos}$). The curves are fitted to data taken from the NACP protocol (43).

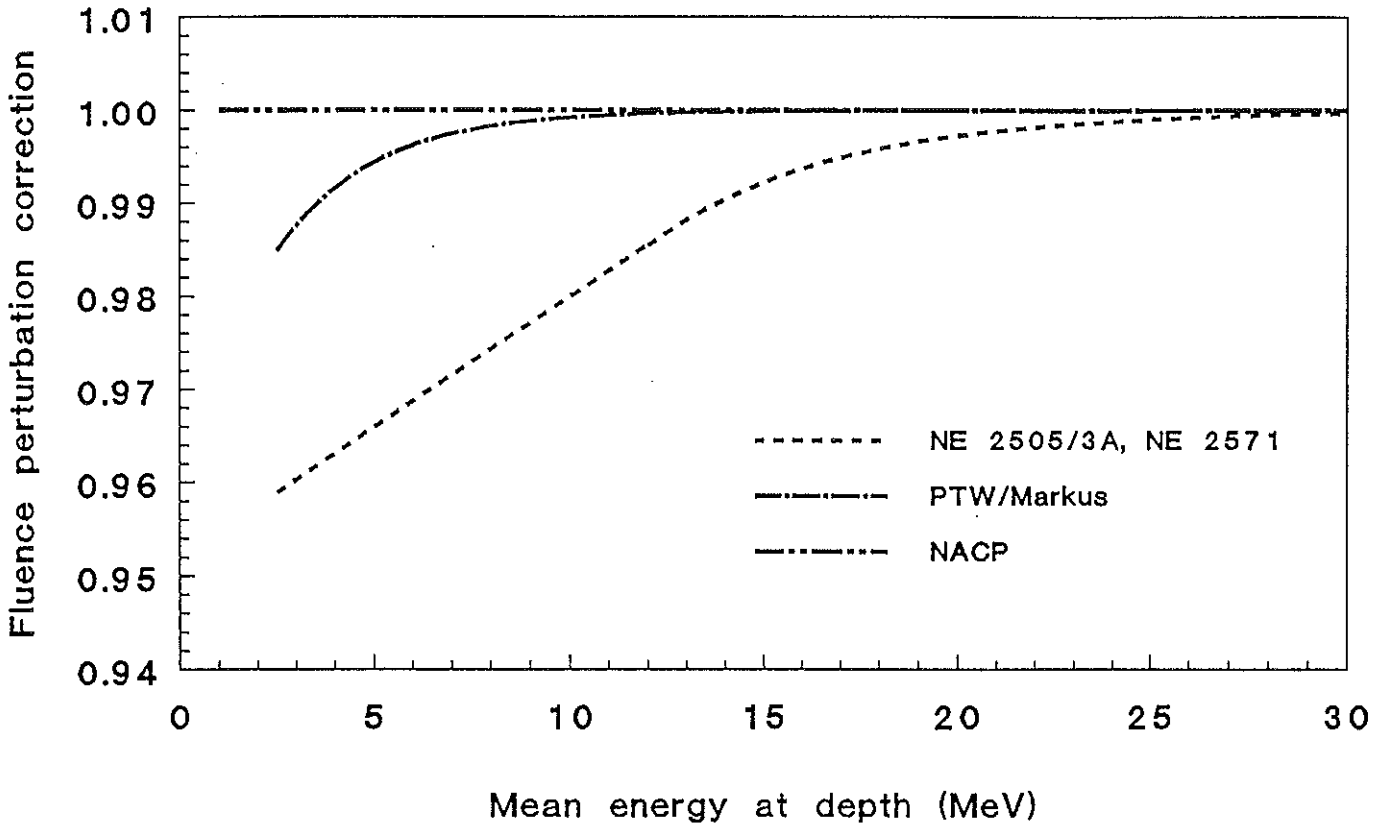

Fig. 3 Fluence perturbation correction factors (p_f) for the reference chambers as function of the mean energy at depth (MeV). The dashed line for the cylindrical chambers (NE 2505/3A and NE 2571) and the dashed-dotted line for the PTW/Markus chamber are fitted to data taken from Wittkämper et al. (64).

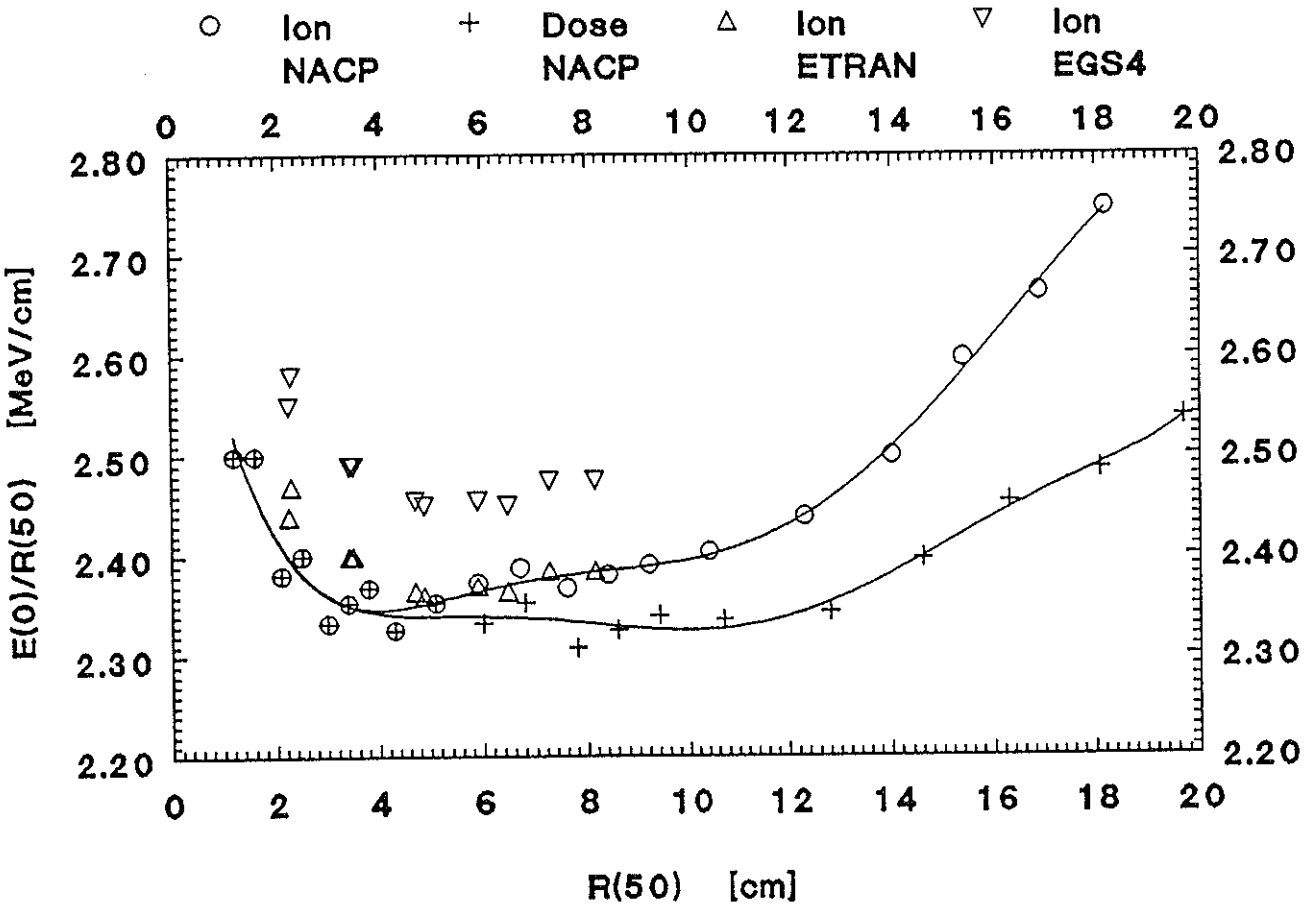

Fig. 4 $\bar{E}_0/R_{50}$ conversion factors (MeV/cm) as function of the R_{50} depth (mm) in water. The circles are values taken from the NACP protocol (42) for R_{50} taken from the depth ionization curve for SSD=100 cm ($R_{50,ion}$). The plus signs are values taken from the NACP protocol for R_{50} taken from the depth-dose curve for SSD=100 cm ($R_{50,dos}$). The triangles are values measured values by Ten Haken et al. (57), based on Monte Carlo calculations with the ETRAN code and the EGS4 code. The two curves are fitted to data taken from the NACP protocol.

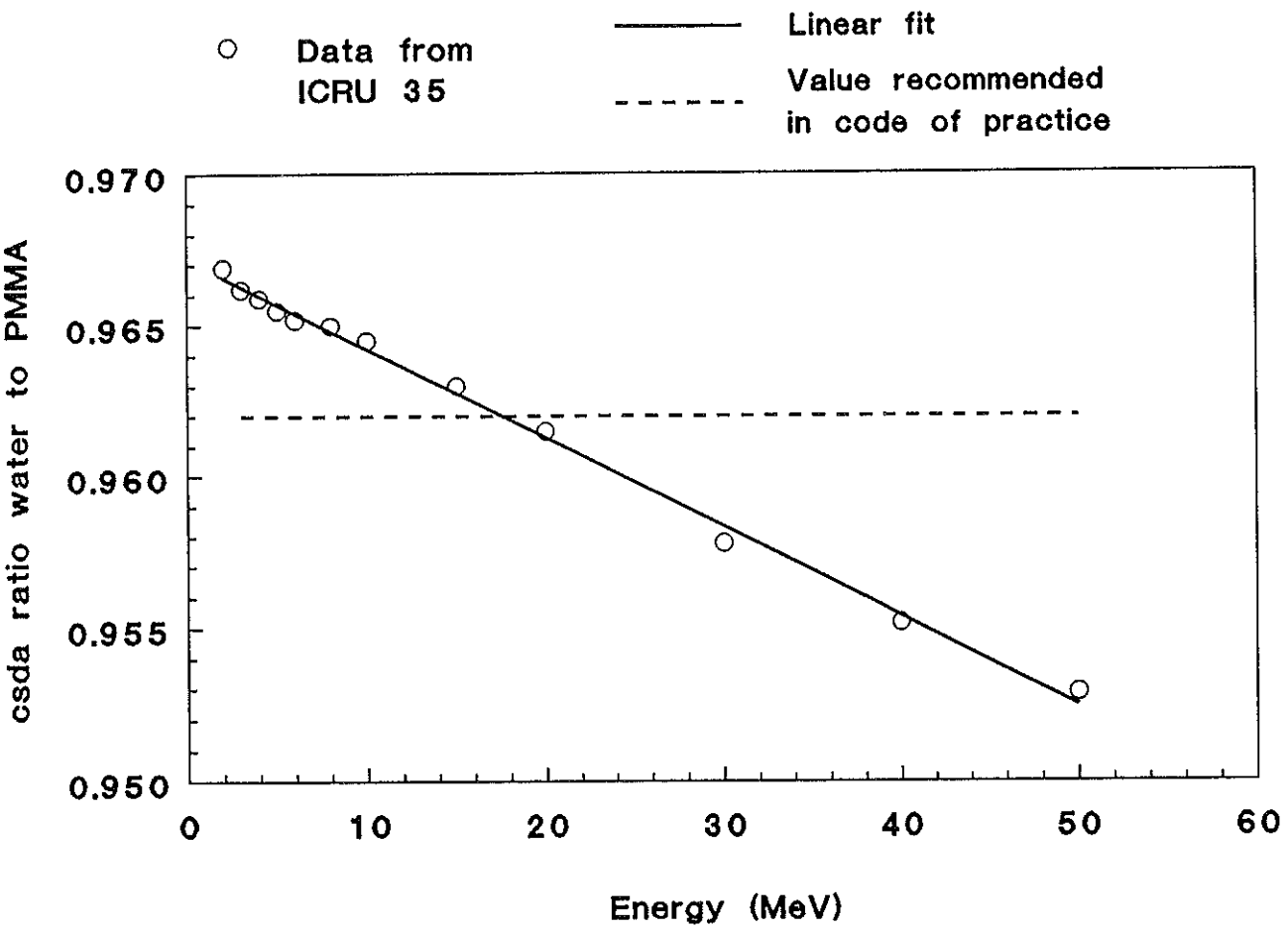

Fig. 5 Continuous-slowing-down-approximation range (csda) ratios water to PMMA as function of the mean energy at the phantom surface (MeV). The csdr ratio multiplied by the density of PMMA (gcm^{-3}) gives the scaling factor by which the depth in PMMA has to be multiplied to obtain the depth in water. Data are taken from ICRU Report 35 (28). The line represents a linear fit based on the least square regression method. For reasons of simplicity a single value of 0.962 has been chosen in this code of practice.

Table I Characteristics of the reference ionization chamber and build-up caps

Ionization chamber		NE 2505/3A	NE 2571		NACP	PTW/Markus
Chamber type		Cylindrical 0.6 cm^3 Farmer	Cylindrical 0.6 cm^3 Farmer		Plane parallel	Plane parallel
Cavity dimensions	length	24 mm	24 mm	plate distance	2 mm	2 mm
	diameter	6.3 mm	6.3 mm	diameter	16.4 mm	5 mm
Chamber wall	material	Graphite	Graphite	window material	Graphite	Polyethylene
	thickness	0.065 gcm^{-2}	0.065 gcm^{-3}	thickness	0.09 gcm^{-2}	2.3 $mgcm^{-2}$
Electrode	material	Aluminium	Aluminium	material	Graphite	Polystyrene
	diameter	1 mm	1 mm	diameter	10 mm	3.5 mm
Build-up cap	material	PMMA	Delrin	material (a)	Graphite	Graphite
	thickness	0.558 gcm^{-2}	0.556 gcm^{-2}	thickness	0.54 gcm^{-2}	0.54 gcm^{-2}
Guard ring				width (mm)	3.2	0.7

(a) A 0.54 gcm^{-2} thick graphite sheet must be used as build-up material

NE : Nuclear Enterprises Ltd.
NACP : Scanditronix, Dosetek (Calcam)
PTW : Physikalisch Technische Werkstätte

Table II Stopping power ratios water to air for mono-energetic electron beams as a function of the mean energy at phantom surface (MeV) and depth (mm). The stopping power ratios are calculated by Berger (1) with collision stopping power values taken from ICRU 37 (29) and Δ = 10 keV.

Depth (mm)	Mean energy at phantom surface (MeV) 3	4	5	6	7	8	9	10	12
0	1.078	1.059	1.040	1.029	1.019	1.011	1.003	0.997	0.986
1	1.081	1.061	1.042	1.030	1.020	1.012	1.005	0.998	0.987
2	1.084	1.064	1.044	1.032	1.022	1.013	1.006	0.999	0.988
3	1.089	1.067	1.046	1.034	1.024	1.015	1.007	1.000	0.989
4	1.093	1.071	1.050	1.036	1.026	1.017	1.009	1.002	0.990
5	1.098	1.075	1.054	1.039	1.028	1.019	1.010	1.003	0.991
6	1.103	1.080	1.058	1.043	1.031	1.021	1.012	1.005	0.993
8	1.113	1.090	1.067	1.050	1.037	1.026	1.016	1.009	0.996
10	1.121	1.099	1.076	1.058	1.043	1.031	1.021	1.013	0.999
12	1.129	1.108	1.085	1.066	1.050	1.037	1.026	1.017	1.002
14	1.133	1.117	1.095	1.075	1.058	1.044	1.032	1.022	1.006
16		1.124	1.104	1.084	1.066	1.050	1.038	1.027	1.010
18		1.130	1.112	1.093	1.074	1.057	1.044	1.032	1.014
20		1.133	1.120	1.101	1.082	1.065	1.050	1.038	1.018
25			1.131	1.120	1.102	1.083	1.067	1.053	1.030
30				1.129	1.119	1.102	1.084	1.069	1.042
35					1.128	1.118	1.102	1.085	1.056
40						1.126	1.116	1.101	1.071
45						1.127	1.125	1.115	1.086
50							1.126	1.123	1.101
60									1.121

Depth (mm)	14	16	18	20	22	25	30	40	50
0	0.977	0.969	0.961	0.955	0.949	0.940	0.928	0.912	0.904
1	0.978	0.969	0.962	0.955	0.949	0.941	0.929	0.913	0.905
2	0.978	0.970	0.963	0.956	0.950	0.942	0.930	0.914	0.906
3	0.979	0.971	0.964	0.957	0.951	0.943	0.931	0.915	0.907
4	0.980	0.972	0.965	0.958	0.952	0.944	0.932	0.916	0.908
5	0.982	0.973	0.966	0.959	0.953	0.945	0.933	0.917	0.909
6	0.983	0.974	0.967	0.960	0.954	0.946	0.934	0.918	0.909
8	0.985	0.976	0.969	0.962	0.956	0.948	0.936	0.920	0.911
10	0.988	0.979	0.971	0.964	0.958	0.950	0.938	0.922	0.913
12	0.991	0.981	0.973	0.966	0.960	0.952	0.940	0.924	0.914
14	0.994	0.984	0.976	0.968	0.962	0.954	0.942	0.925	0.916
16	0.997	0.987	0.978	0.971	0.965	0.956	0.944	0.927	0.917
18	1.001	0.990	0.981	0.973	0.967	0.957	0.945	0.929	0.918
20	1.004	0.993	0.983	0.975	0.969	0.959	0.947	0.930	0.920
25	1.013	1.000	0.990	0.981	0.974	0.964	0.952	0.934	0.923
30	1.023	1.008	0.997	0.987	0.980	0.969	0.956	0.938	0.926
35	1.034	1.017	1.004	0.994	0.986	0.974	0.960	0.941	0.929
40	1.046	1.027	1.012	1.001	0.992	0.979	0.964	0.944	0.932
45	1.059	1.037	1.021	1.008	0.999	0.985	0.969	0.948	0.935
50	1.072	1.049	1.030	1.016	1.006	0.990	0.973	0.951	0.938
60	1.100	1.074	1.051	1.033	1.021	1.002	0.983	0.958	0.943
80	1.120	1.116	1.098	1.076	1.058	1.032	1.005	0.972	0.954
100			1.116	1.112	1.094	1.068	1.032	0.990	0.966
120						1.103	1.062	1.009	0.980
140						1.107	1.095	1.031	0.996
160							1.103	1.056	1.013
180								1.080	1.031
200								1.094	1.051
220									1.070
240									1.082

Table III-a $C_{w,e}$ conversion factors for the **NE 2505/3A** and **NE 2571** ionization chambers as a function of the mean energy at phantom surface (MeV) and depth (mm) in water.

Depth (mm)	Mean energy at phantom surface (MeV)								
	3	4	5	6	7	8	9	10	12
0	1.023	1.008	0.992	0.985	0.978	0.973	0.968	0.965	0.960
1	1.025	1.009	0.994	0.985	0.978	0.973	0.970	0.966	0.960
2	1.027	1.011	0.995	0.986	0.980	0.974	0.970	0.966	0.961
3		1.013	0.996	0.988	0.981	0.975	0.970	0.966	0.961
4		1.017	0.999	0.989	0.982	0.976	0.971	0.967	0.961
5		1.021	1.002	0.991	0.983	0.978	0.972	0.968	0.962
6		1.024	1.005	0.994	0.986	0.979	0.973	0.969	0.963
8			1.012	0.999	0.990	0.982	0.975	0.972	0.964
10			1.019	1.005	0.994	0.986	0.979	0.974	0.966
12				1.012	0.999	0.990	0.982	0.976	0.968
14				1.019	1.005	0.995	0.987	0.980	0.970
16					1.012	0.999	0.991	0.983	0.973
18					1.018	1.005	0.995	0.987	0.975
20						1.011	0.999	0.991	0.977
25							1.012	1.002	0.986
30								1.014	0.994
35									1.004
40									1.016

	14	16	18	20	22	25	30	40	50
0	0.956	0.951	0.945	0.941	0.936	0.928	0.916	0.901	0.893
1	0.956	0.951	0.946	0.941	0.936	0.929	0.917	0.902	0.894
2	0.956	0.952	0.947	0.942	0.937	0.930	0.918	0.903	0.895
3	0.956	0.952	0.948	0.942	0.938	0.931	0.919	0.904	0.896
4	0.957	0.953	0.948	0.943	0.939	0.931	0.920	0.905	0.897
5	0.958	0.953	0.949	0.944	0.940	0.932	0.921	0.906	0.898
6	0.959	0.954	0.950	0.945	0.940	0.933	0.922	0.907	0.898
8	0.959	0.955	0.951	0.946	0.942	0.935	0.924	0.909	0.900
10	0.961	0.957	0.953	0.948	0.944	0.937	0.926	0.911	0.902
12	0.962	0.958	0.954	0.949	0.946	0.939	0.928	0.913	0.903
14	0.964	0.960	0.956	0.951	0.947	0.940	0.930	0.914	0.905
16	0.966	0.961	0.957	0.953	0.949	0.942	0.932	0.916	0.906
18	0.968	0.963	0.959	0.955	0.950	0.943	0.933	0.918	0.907
20	0.970	0.964	0.960	0.956	0.952	0.945	0.935	0.919	0.909
25	0.975	0.968	0.963	0.959	0.956	0.949	0.939	0.922	0.912
30	0.981	0.972	0.967	0.962	0.959	0.953	0.943	0.926	0.915
35	0.988	0.977	0.970	0.966	0.963	0.956	0.946	0.929	0.918
40	0.997	0.984	0.975	0.970	0.966	0.959	0.949	0.932	0.921
45	1.007	0.990	0.980	0.973	0.969	0.963	0.953	0.936	0.924
50	1.017	0.999	0.986	0.978	0.973	0.965	0.956	0.939	0.926
60		1.018	1.001	0.988	0.981	0.970	0.963	0.945	0.931
80				1.020	1.007	0.988	0.973	0.956	0.942
100						1.015	0.989	0.969	0.952
120							1.010	0.978	0.964
140								0.990	0.974
160								1.007	0.982
180								1.025	0.992
200									1.005
220									1.018
240									1.025

Table III-b $C_{w,e}$ conversion factors for the **NACP** ionization chamber as a function of the mean energy at phantom surface (MeV) and depth (mm) in water.

Depth (mm)	Mean energy at phantom surface (MeV)								
	3	4	5	6	7	8	9	10	12
0	1.052	1.034	1.015	1.004	0.995	0.987	0.979	0.973	0.962
1	1.055	1.036	1.017	1.005	0.996	0.988	0.981	0.974	0.963
2	1.058	1.039	1.019	1.007	0.998	0.989	0.982	0.975	0.964
3	1.063	1.041	1.021	1.009	0.999	0.991	0.983	0.976	0.965
4	1.067	1.045	1.025	1.011	1.001	0.993	0.985	0.978	0.966
5	1.072	1.050	1.029	1.014	1.003	0.995	0.986	0.979	0.967
6	1.077	1.054	1.033	1.018	1.006	0.997	0.988	0.981	0.969
8	1.086	1.064	1.041	1.025	1.012	1.001	0.992	0.985	0.972
10	1.094	1.073	1.050	1.033	1.018	1.006	0.997	0.989	0.975
12	1.102	1.081	1.059	1.040	1.025	1.012	1.001	0.993	0.978
14	1.106	1.090	1.069	1.049	1.033	1.019	1.007	0.998	0.982
16		1.097	1.078	1.058	1.040	1.025	1.013	1.002	0.986
18		1.103	1.085	1.067	1.048	1.032	1.019	1.007	0.990
20		1.106	1.093	1.075	1.056	1.039	1.025	1.013	0.994
25			1.104	1.093	1.076	1.057	1.041	1.028	1.005
30				1.102	1.092	1.076	1.058	1.043	1.017
35					1.101	1.091	1.076	1.059	1.031
40						1.099	1.089	1.075	1.045
45						1.100	1.098	1.088	1.060
50							1.099	1.096	1.075
55								1.098	1.086
60									1.094

Depth (mm)	14	16	18	20	22	25	30	40	50
0	0.954	0.946	0.938	0.932	0.926	0.917	0.906	0.890	0.882
1	0.955	0.946	0.939	0.932	0.927	0.918	0.907	0.891	0.883
2	0.955	0.947	0.940	0.933	0.928	0.919	0.908	0.892	0.884
3	0.956	0.948	0.941	0.934	0.929	0.920	0.909	0.893	0.885
4	0.957	0.949	0.942	0.935	0.930	0.921	0.910	0.894	0.886
5	0.958	0.950	0.943	0.936	0.931	0.922	0.911	0.895	0.887
6	0.959	0.951	0.944	0.937	0.932	0.923	0.912	0.896	0.887
8	0.961	0.953	0.946	0.939	0.933	0.925	0.914	0.898	0.889
10	0.964	0.956	0.948	0.941	0.935	0.927	0.916	0.900	0.891
12	0.967	0.957	0.950	0.943	0.937	0.929	0.917	0.902	0.892
14	0.970	0.960	0.953	0.945	0.939	0.931	0.919	0.903	0.894
16	0.973	0.963	0.955	0.948	0.942	0.933	0.921	0.905	0.895
18	0.977	0.966	0.957	0.950	0.943	0.934	0.922	0.907	0.896
20	0.980	0.969	0.959	0.952	0.945	0.936	0.924	0.908	0.898
25	0.989	0.976	0.966	0.957	0.951	0.941	0.929	0.912	0.901
30	0.998	0.984	0.973	0.963	0.956	0.946	0.933	0.916	0.904
35	1.009	0.993	0.980	0.970	0.962	0.951	0.937	0.918	0.907
40	1.021	1.002	0.988	0.977	0.968	0.956	0.941	0.921	0.910
45	1.034	1.012	0.997	0.984	0.975	0.961	0.946	0.925	0.913
50	1.046	1.024	1.005	0.992	0.982	0.966	0.950	0.928	0.916
55	1.060	1.036	1.015	0.999	0.989	0.972	0.955	0.931	0.917
60	1.074	1.048	1.026	1.008	0.996	0.978	0.959	0.935	0.920
80	1.093	1.089	1.072	1.050	1.033	1.007	0.981	0.949	0.931
100			1.089	1.085	1.068	1.042	1.007	0.966	0.943
120						1.077	1.037	0.985	0.957
140						1.080	1.069	1.006	0.972
160							1.077	1.031	0.989
180								1.054	1.006
200								1.068	1.026
220									1.044
240									1.056

Table III-c Cw,e conversion factors for the **PTW/Markus** ionization chamber as a function of the mean energy at phantom surface (MeV) and depth (mm) in water.

Depth (mm)	Mean energy at phantom surface (MeV)								
	3	4	5	6	7	8	9	10	12
0	1.054	1.040	1.024	1.015	1.006	0.999	0.992	0.986	0.976
1	1.056	1.041	1.025	1.016	1.007	1.000	0.994	0.987	0.977
2	1.057	1.043	1.027	1.017	1.009	1.001	0.995	0.988	0.978
3		1.045	1.028	1.019	1.010	1.003	0.995	0.989	0.979
4		1.048	1.031	1.020	1.012	1.004	0.997	0.991	0.980
5		1.051	1.034	1.023	1.014	1.006	0.998	0.992	0.981
6		1.055	1.037	1.026	1.016	1.008	1.000	0.994	0.983
8			1.044	1.031	1.021	1.012	1.003	0.997	0.985
10			1.049	1.037	1.026	1.016	1.008	1.001	0.988
12				1.043	1.031	1.021	1.012	1.004	0.991
14				1.049	1.037	1.027	1.017	1.009	0.995
16					1.043	1.031	1.022	1.013	0.998
18					1.048	1.036	1.027	1.017	1.002
20						1.042	1.031	1.022	1.005
25							1.044	1.034	1.016
30								1.045	1.025
35									1.036
40									1.047

	14	16	18	20	22	25	30	40	50
0	0.967	0.959	0.951	0.945	0.940	0.931	0.919	0.903	0.895
1	0.968	0.959	0.952	0.945	0.940	0.932	0.920	0.904	0.896
2	0.968	0.960	0.953	0.946	0.941	0.933	0.921	0.905	0.897
3	0.969	0.961	0.954	0.947	0.942	0.934	0.922	0.906	0.898
4	0.970	0.962	0.955	0.948	0.943	0.935	0.923	0.907	0.899
5	0.972	0.963	0.956	0.949	0.944	0.936	0.924	0.908	0.900
6	0.973	0.964	0.957	0.950	0.945	0.937	0.925	0.909	0.900
8	0.975	0.966	0.959	0.952	0.947	0.939	0.927	0.911	0.902
10	0.978	0.969	0.961	0.954	0.949	0.941	0.929	0.913	0.904
12	0.981	0.971	0.963	0.956	0.951	0.942	0.931	0.915	0.905
14	0.984	0.974	0.966	0.958	0.953	0.944	0.933	0.916	0.907
16	0.986	0.977	0.968	0.961	0.955	0.946	0.935	0.918	0.908
18	0.990	0.980	0.971	0.963	0.957	0.947	0.936	0.920	0.909
20	0.993	0.983	0.973	0.965	0.959	0.949	0.938	0.921	0.911
25	1.001	0.989	0.980	0.971	0.964	0.954	0.943	0.925	0.914
30	1.010	0.997	0.986	0.977	0.970	0.959	0.946	0.929	0.917
35	1.019	1.005	0.993	0.984	0.976	0.964	0.950	0.932	0.920
40	1.029	1.013	1.000	0.990	0.982	0.969	0.954	0.935	0.923
45	1.038	1.022	1.008	0.997	0.988	0.975	0.959	0.939	0.926
50	1.047	1.031	1.016	1.004	0.995	0.980	0.963	0.942	0.929
60		1.049	1.033	1.019	1.008	0.991	0.973	0.948	0.934
80				1.051	1.040	1.018	0.994	0.962	0.944
100						1.046	1.019	0.980	0.956
120							1.042	0.998	0.970
140								1.018	0.986
160								1.039	1.002
180								1.056	1.019
200									1.036
220									1.050
240									1.055

Table IV Summary of calculated and measured values of $k_{att} * k_m$ for the reference ionization chambers and build-up caps.

Ionization chamber	Calculated	Measured			Value used in this code of practice
		Wittkämper et al. (62,63)	Johansson (32)	Mattsson et al. (40)	
NE 2505/3A	0.980	0.980	0.986		0.983
NE 2571	0.985	0.980			0.983
NACP		0.980		0.978*	0.979
PTW/Markus		0.993			0.993

* renormalized

Table V The quadratic fit coefficients for pulsed (A) and pulsed-swept (B) radiation as a function of the voltage ratio V_1/V_2. Data are taken from Weinhous and Meli (61).

A

Pulsed beams - Quadratic fit coefficients			
Voltage ratio	a_0	a_1	a_2
2.0	2.337	-3.636	2.299
2.5	1.474	-1.587	1.114
3.0	1.198	-0.8753	0.6773
3.5	1.080	-0.5421	0.4627
4.0	1.022	-0.3632	0.3413
5.0	0.9745	-0.1875	0.2153
6.0	0.9584	-0.1075	0.1495
8.0	0.9502	-0.03732	0.08750
10.0	0.9516	-0.01041	0.05909

B

Pulsed swept beams - Quadratic fit coefficients			
Voltage ratio	a_0	a_1	a_2
2.0	4.711	-8.242	4.533
2.5	2.719	-3.977	2.261
3.0	2.001	-2.402	1.404
3.5	1.665	-1.647	0.9841
4.0	1.468	-1.200	0.7340
5.0	1.279	-0.7500	0.4741
6.0	1.177	-0.5081	0.3342
8.0	1.089	-0.2890	0.2020
10.0	1.052	-0.1896	0.1398